JACS
JOURNAL OF THE AMERICAN CHEMICAL SOCIETY
pubs.acs.org/JACS
Article

Charge Separation from an Intra-Moiety Intermediate State in the High-Performance PM6:Y6 Organic Photovoltaic Blend

Rui Wang, Chunfeng Zhang,* Qian Li, Zhiguo Zhang, Xiaoyong Wang, and Min Xiao

Cite This: J. Am. Chem. Soc. 2020, 142, 12751−12759
Read Online

ABSTRACT: Bulk-heterojunction organic photovoltaic devices with nonfullerene acceptors (NFAs) exhibit efficient hole transfer with small interfacial energy offset, which results in power conversion efficiencies above 17% in single junction devices using the high-performance NFA of Y6. However, the underlying mechanism responsible for the hole transfer channel in the polymer/Y6 blends remains poorly understood. Herein, we report that the hole transfer channel of photocharge generation is mediated by an intra-moiety excited state in a blend of donor polymer PM6 and NFA Y6 using broadband transient absorption (TA) spectroscopy. By comparing the TA data recorded from the solution and film Y6 samples, we identify the ultrafast formation of an intra-moiety excimer state together with the conversion from the primary local excitation on a time scale of ∼0.2 ps in the Y6 film. The intra-moiety excimer state acts as the intermediate for the hole transfer channel, which dissociates into free polarons on a time scale of ∼15 ps in the PM6/Y6 blend at room temperature. The intra-moiety intermediate state, arising from the intermolecular coupling in Y6 domains, is markedly different from the interfacial charge transfer state, which is commonly accepted as the intermediate state for the electron transfer channel. These findings suggest that manipulating the interplay between intra-moiety and interfacial excited species can provide a promising route for further improving device performance.

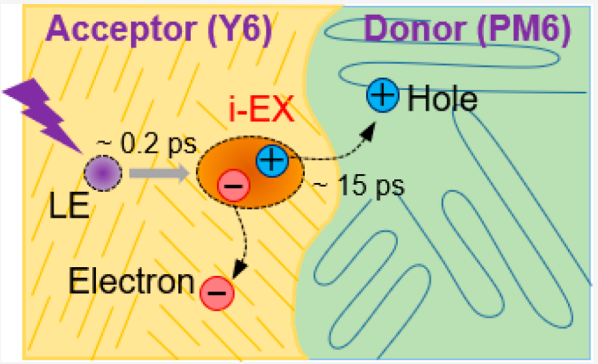

INTRODUCTION

The performance of organic photovoltaic (OPV) devices has dramatically improved in the past few years, having achieved certified power conversion efficiency of above 17%,[1] which has benefited from the rapid development of nonfullerene acceptors (NFAs).[2−17] In OPV blends, charge generation is accomplished using bulk heterojunctions of electron donors and acceptors, whereas charge transfer occurs at the donor/acceptor interfaces.[18−22] For decades, fullerene and its derivatives have been widely employed as electron acceptors, while electron transfer from polymer donors is considered as the major channel for photocurrent generation.[23−33] NFAs show strong absorption in the visible to near-infrared wavelength range, which significantly extends the solar spectral coverage beyond those of OPV systems with fullerene acceptors.[12−14] Hole transfer from excitation in NFAs makes an equivalent contribution to that of electron transfer from the polymer donor to charge generation in OPV blends with NFAs.[9,34,35] Remarkably, hole transfer is highly efficient in multiple NFA systems with small interfacial energy offsets between the highest occupied molecular orbital (HOMO) levels of donors and acceptors, which enables low voltage loss and high charge generation efficiency in these devices.[6,16,36,37] However, the specific processes underlying such hole transfer channel and the subsequent charge separation remain poorly understood in high-performance OPV blends with different nonfullerene acceptors.

Charge separation in OPV blends has been studied extensively in polymer/fullerene systems.[21] Charge separation is widely considered to be a two-step process, as (i) the photoexcited Frenkel-type local excitation (LE) state in the polymer donor undergoes electron transfer at the donor/acceptor interface, to create an intermediate interfacial charge transfer (xCT) state; and (ii) the bound xCT state further dissociates into a charge-separated (CS) state of free polarons, as collected by electrodes. Together with other effects, including vibronic coupling,[38] charge delocalization,[29,30] "hot" carrier transfer,[39] and entropy-driven processes,[40−42] such an xCT state-mediated scheme well explains the charge generation dynamics in various polymer/fullerene systems. This scenario has also been applied to interpret hole transfer with the xCT state as the intermediate step for charge separation. Most high-performance NFAs are small molecules

Received: May 4, 2020
Published: June 30, 2020

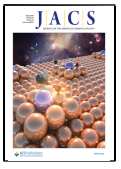

https://dx.doi.org/10.1021/jacs.0c04890
J. Am. Chem. Soc. 2020, 142, 12751−12759

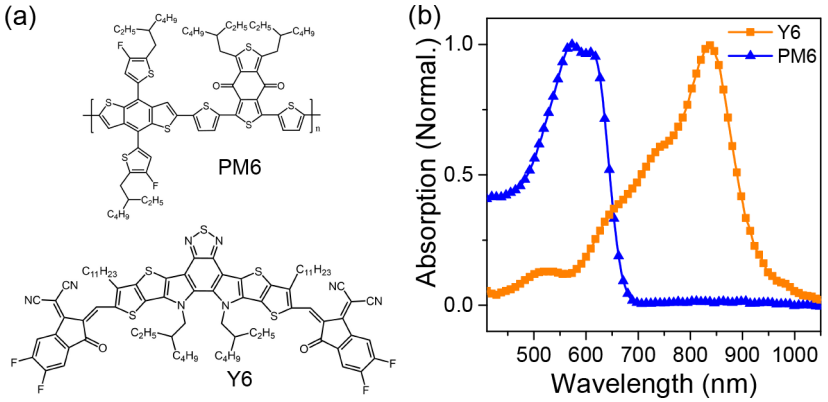

Figure 1. (a) Molecular structures and (b) absorption spectra of polymer donor PM6 and small-molecule acceptor Y6.

with two-dimensional architectures, in which strongly electron-deficient end groups are attached to a fused-ring conjugated core bearing out-of-plane substituents.[12] Molecular interactions in condensed-phase NFAs might result in excited states with different degrees of CT character, as configured by electron and hole wave functions delocalized over different acceptor molecules at the same moiety.[43−45] These intra-moiety excited (i-EX) states are similar to excited species with CT characters quoted as the excimer,[46,47] pseudo CT,[48] or polaron pair states in polymers.[49−52] Whether and how such i-EX states in NFAs are involved in the dynamics of charge generation in polymer/NFA blends remains to be explored.

In this work, we report the identification of an i-EX state as the intermediate of hole transfer channel for charge separation in a prototypical OPV blend with state-of-the-art NFA Y6. The embedding of an electron-deficient group on the central π-conjugated core in Y6 creates a strong near-infrared light absorber along with high crystallinity. Y6-based OPV devices are among the best performance with broadband photo response and markedly low energy loss. Using broadband transient absorption (TA) spectroscopy, we monitor the carrier dynamics of electron and hole transfer channels with a temporal resolution of <30 fs. The excited-state absorption (ESA) feature of the intermediate i-EX state at 1550 nm in the Y6 film is identified. Upon selective excitation of Y6, the photoexcited LE state is converted into the i-EX state on a time scale of ∼0.2 ps in the PM6/Y6 blend film. The i-EX state dissociates into the CS state of free polarons on a time scale of ∼15 ps without involving the interfacial xCT state. This intra-moiety-state-mediated hole transfer channel of charge separation is substantially different from the xCT state-mediated electron transfer channel in the PM6/Y6 blends. Formation of the intermediate i-EX state is insusceptible to the interfacial driving energy, which explains the efficient hole transfer upon small HOMO energy offset. This work highlights the pivotal role played by the i-EX state in charge generation dynamics in polymer/NFA blends, which indicates an alternative strategy to optimize device performance by manipulating the interplay between excited species of LE, i-EX, and xCT in polymer/NFA blends.

MATERIALS AND METHODS

Sample Preparation. The OPV blend consists of polymer donor PM6 and small-molecule acceptor Y6, with their molecular structures shown in Figure 1a. Polymer donor PM6 is a fluorinated medium bandgap polymer based on the benzodithiophene-*alt*-benzo[1,2-*b*:4,5-*c*′]dithiophene-4,8-dione backbone, while small-molecule NFA Y6 contains an electron-deficient centrally fused conjugated ring (dithienthiophen[3.2-*b*]-pyrrolobenzothiadiazole) flanked with 2-(5,6-difluoro-3-oxo-2,3-dihydro-1*H*-inden-1-ylidene)malononitrile end-capping units. The PM6/Y6 system shows excellent performance that has been well reproduced by different groups, with power conversion efficiencies of ∼16% or above.[5,6,53,54] The power conversion efficiencies of the organic solar cells using the same active layers reach ∼17% as shown in Figure S1. These chemicals were purchased from Solarmer Materials Inc. Spin coating was used to prepare the film samples for optical experiments. The PM6/Y6 blend samples were prepared with a 1:1.2 mass ratio of donor and acceptor at a total concentration of 16 mg/mL,[5] which resulted in film samples with thicknesses of ∼150 nm. The neat films of Y6 and PM6 are prepared by spin coating using the chloroform solutions of concentrations of 8 mg/mL. The film samples were annealed under an argon atmosphere at 110 °C for 10 min. Chlorobenzene solution samples of Y6 were also prepared at a concentration of 80 μg/mL for reference to study the dynamics of LE at the Y6 molecule (Figure S2).

The optical absorption spectra of polymer donor PM6 and small-molecule acceptor Y6 are complementary in the visible to near-infrared range (Figure 1b). From cyclic voltammetry measurements, the HOMO level of PM6 (−5.56 eV) is about 0.09 eV higher than that of Y6 (−5.65 eV), while the lowest unoccupied molecular orbital (LUMO) offset is about 0.6 eV at the donor/acceptor interface.[5]

Time-Resolved Spectroscopy. Ultrafast broadband TA spectroscopy was conducted using a Ti:sapphire regenerative amplifier (Libra, Coherent Inc.) operating at a repetition rate of 5 kHz. A homemade noncollinear optical parametric amplifier (OPA) pumped by the regenerative amplifier was used to generate the pump beam. According to the absorption spectra (Figure 1b), the wavelengths of the pump pulses were tuned to be centered at 750 and 550 nm for selectively exciting acceptor and donor, respectively (Figures S2 and S3). To make the noncollinear OPA operating near 750 nm, an optical filter (BG 39, Schott glass 1 mm thick) was used to optimize the spectral coverage of seeded supercontinuum. The white light supercontinuum was employed as the probe light source. In the infrared range of >1000 nm, the probe beam was generated by focusing a small portion of the fundamental beam at 800 nm onto a 5 mm-thick plate of yttrium aluminum garnet (YAG). In the wavelength range of 600−1000 nm, the probe light was generated by focusing the output beam at 1300 nm from a homemade OPA onto a 3 mm sapphire plate. Pulse-to-pulse balanced detection was employed to reduce the noise caused by infrared supercontinuum instability. The supercontinuum light was split into two beams for balanced detection. The probe and reference beams were then routed to a double line InGaAs camera (G11608, Hamamatsu) mounted on a monochromator (Acton 2358, Princeton Instrument). Pulse-to-pulse spectral analysis was conducted at 5 kHz using a homemade field-programmable gate array (FPGA) control board. The signal-to-noise ratio ($\Delta T/T$) was $<10^{-5}$ after 10 000 pump-on and pump-off shots were averaged for each data point. The group velocity dispersions of the pump and probe beams were compressed by

https://dx.doi.org/10.1021/jacs.0c04890
J. Am. Chem. Soc. 2020, 142, 12751−12759

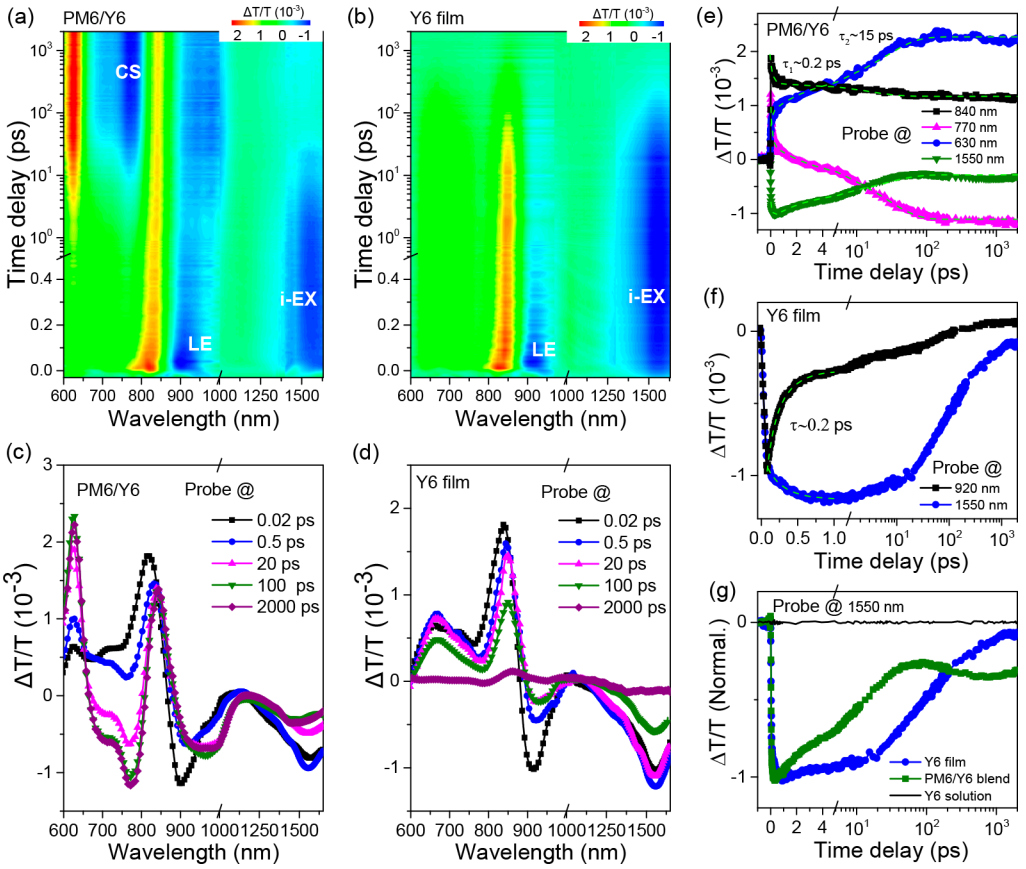

Figure 2. Hole transfer from the i-EX state in the blend PM6/Y6 film. (a,b) Broadband TA data of the (a) PM6/Y6 blend and (b) neat Y6 films with pump at 750 nm. TA spectra from the two samples at different time delays are shown in (c) and (d). (e) TA traces probed at different wavelengths from the PM6/Y6 blend film. (f) TA traces of ESA signals probed at 920 and 1550 nm recorded from the neat Y6 film. (g) Normalized TA traces probed at 1550 nm recorded from blend PM6/Y6 and neat Y6 films. No signal was detected in Y6 solution in the probe wavelength range near 1550 nm (Figure S6). LE, local excitation; i-EX, intra-moiety excited state; CS, charge-separated state.

combining chirp mirrors and wedge pairs. The temporal duration of pump pulse is diagnosed by the fringe-resolved autocorrelator (Figure S3). The overall temporal resolution was <30 fs. The relative polarization difference of the pump and probe beams was set at the magic angle. During TA measurements, the samples were kept in nitrogen to avoid photodegradation. As checked by pump-fluence-dependent experiments (Figure S4), the decay dynamics in the Y6 and PM6 films are nearly independent of pump fluence in the weak pump regime (<2 μJ/cm^2). The pump fluence was kept at <2 μJ/cm^2, unless otherwise specified, to minimize the exciton−exciton annihilation effect.

The spectrum of photoinduced absorption (PIA) upon continuous wave (cw) excitation was measured to determine the spectral features of the CS state. For PIA measurements, the pump light was replaced with a cw He−Ne laser at 632.8 nm modulated at 2.5 kHz. The pump fluence was set at 60 mW/cm^2 at the same level of pump density of AM 1.5 in the visible range.

RESULTS

Hole Transfer Channel for Charge Separation. Figure 2 shows the TA data recorded from the blend PM6/Y6 and neat Y6 films when acceptor Y6 was selectively excited at 750 nm. In the blend film, temporal evolution exhibits a two-step spectral transfer dynamics involving three excited species (Figure 2a). Simultaneously upon optical pumping, the primary excitation of Y6 is observed with a bleach band centered at 830 nm and an ESA band centered at 920 nm (Figure 2a). In addition, a feature ESA centered at 1550 nm appears upon optical pump and increases in the first 500 fs with a lifetime of ~0.2 ps (Figure 2c). The ESA signal at 1550 nm decays with a lifetime of ~15 ps, which exhibits second-stage spectral transfer with the onset of an additional ESA feature at 770 nm and a bleach signal near 630 nm. Emergence of the bleach signal near the absorption peak of PM6 is induced by hole transfer from Y6 to PM6. The resulting excited species persists to a much longer time scale of >2 ns without significant decay (Figure 2e). To illustrate the hole transfer mechanism, elucidating the microscopic nature of the different excited states is essential.

First, we attempt to understand the resulting long-lived state in the blend PM6/Y6 film. The coexistence of ground-state bleaching (GSB) signals for both donor PM6 and acceptor Y6 suggests that excitations occupied the acceptor and electron sites. This configuration is possibly the bound interfacial xCT state or the CS state of free polarons. To distinguish these two species, we acquire the spectral features of the CS state by recording PIA spectra with weak cw excitation. The lifetime of the CS state of free polarons is orders of magnitude longer than that of the bounded excited species. As established in the literature, upon weak cw excitation, the PIA signal is primarily induced by the long-lived CS state.[31,55−57] The PIA spectrum of the PM6/Y6 blend agrees well with the TA spectrum of the long-lived excited state with two ESA features at 770 and 980 nm. While the ESA at 980 nm is entangled with the spectral feature of the bounded excited state at the early stage, the ESA at 770 nm is mainly observed at the late stage, which is likely to

https://dx.doi.org/10.1021/jacs.0c04890
J. Am. Chem. Soc. 2020, 142, 12751−12759

be the positive polarons due to hole transfer from acceptor Y6 to polymer donor PM6. The similarity of these two spectra suggests that free charges are readily generated and manifested as the second-stage spectral transfer with a lifetime of ~15 ps (Figure 3a). Assignment of the CS state is further confirmed by

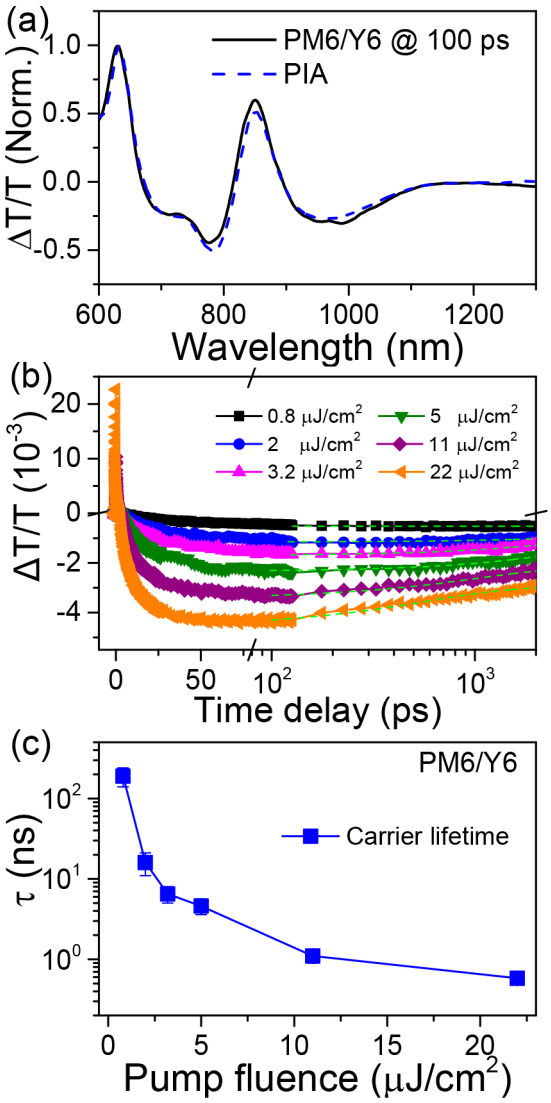

Figure 3. Spectral characteristics of the CS state of free polarons. (a) TA spectrum of PM6/Y6 recorded at 100 ps as compared to PIA spectrum of the CS state upon weak cw excitation. The similarity of these two spectra suggests that the long-lived state is the CS state of free polarons. Pump-fluence dependent (b) TA traces probed at 770 nm and (c) decay lifetimes extracted by an exponential fit. The fluence dependence of decay lifetime is characteristic behavior for bimolecular recombination of free polarons for the CS state.

using excitation fluence-dependent measurements. The decay dynamics probed at 770 nm (Figures 3b and S5) and 980 nm (Figure S5) show strong fluence dependence (Figure 3c), as caused by the bimolecular recombination of free polarons for the CS state.[58] Charge separation is manifested as the second-stage spectral transfer process in the PM6/Y6 blend film.

Intra-Moiety Intermediate State. The above results show that charge separation from the primary excitation at Y6 to the CS state involves an intermediate state. In polymer/fullerene systems, the intermediate state is an interfacial CT state with electrons and holes localized separately at acceptor and donor sites. However, the intermediate state for the hole transfer channel of charge separation in the blend PM6/Y6 film is not an interfacial state. The intermediate state is characterized by the ESA signal at 1550 nm, which is also observed in the neat Y6 film. Early stage optical transfer from the primary excitation at Y6 to the intermediate state is explicitly observed in the neat Y6 film (Figure 2c and d). These results suggest that the intermediate state is an intra-moiety excitation with both electrons and holes localized at Y6 molecules of the same moiety.

To obtain further insight into the intermediate i-EX state, we compare the results for the film and the reference solution sample of Y6 (Figure S6). The primary excitation of the film is a Frenkel-type LE state with an ESA feature similar to that of the LE state in the solution sample (Figure S6). However, the intermediate state feature is not observed in the solution of Y6, which implied that the molecular packing of Y6 molecules is essential for the intermediate i-EX state in the Y6 film. Experimental characterization and quantum chemical computation suggest that Y6 molecules in the film tend to form lamellar packing of Y6 dimers.[59−61] Molecular interaction in the dimers probably stabilizes the i-EX states with different degrees of LE and CT characters. Furthermore, the shift between emission and absorption spectra is more significant in the Y6 film as compared to that in the solution (Figure S2),[62,63] which indicates a larger nuclear displacement for the excited state with CT character in the Y6 film. The strong hybridization between these excited species allows the formation of a portion of i-EX state within the pulse duration, while the delayed rise in the kinetics is contributed by the conversion from the LE to i-EX states characterized with a lifetime of ~0.2 ps. The internal vibrational relaxation may also cause the dynamics on a similar time scale, which can be safely excluded here by the pump-wavelength dependent measurements (Figure S7). When the pump spectrum is tuned to cover the long wavelength tail of Y6 absorption only, the internal vibrational relaxation is largely reduced. With pump wavelength centered at 910 nm, the dynamics probed at the characteristic wavelengths are similar to those pumped at 750 nm (Figure S7), which suggests an unimportant role played by vibrational relaxation. These results suggest that the first step in the hole transfer channel of charge separation is the conversion from the LE to i-EX states in the Y6 moiety.

In the neat Y6 film, the characteristic lifetime is ~0.2 ps for the conversion from LE to i-EX states (Figure 2f). The conversion rates in the blend PM6/Y6 and neat Y6 films are similar, which confirms that the LE state at the acceptor is converted to the i-EX state prior to hole transfer to donor PM6. In contrast, the decay dynamics of the i-EX state is markedly accelerated in the blend film, with the lifetime shortened from ~100 to ~15 ps in the neat Y6 film (Figure 2g). The CS state species emerges on the same time scale. These results suggest that the i-EX state, instead of the xCT state, is the intermediate step for charge separation upon optical excitation at Y6 in the PM6/Y6 blend film. The dynamics of hole transfer channel can be summarized as LE → i-EX → CS for charge separation in the blend film. We checked the hole transfer dynamics in the PM6/Y6 blend films before and after thermal annealing at 110 °C (Figure S8). The dynamics of hole transfer remains basically unchanged after annealing, which implied the hole transfer dynamics is less sensitive to the blend morphology in the PM6/Y6 blend as

https://dx.doi.org/10.1021/jacs.0c04890
J. Am. Chem. Soc. 2020, 142, 12751−12759

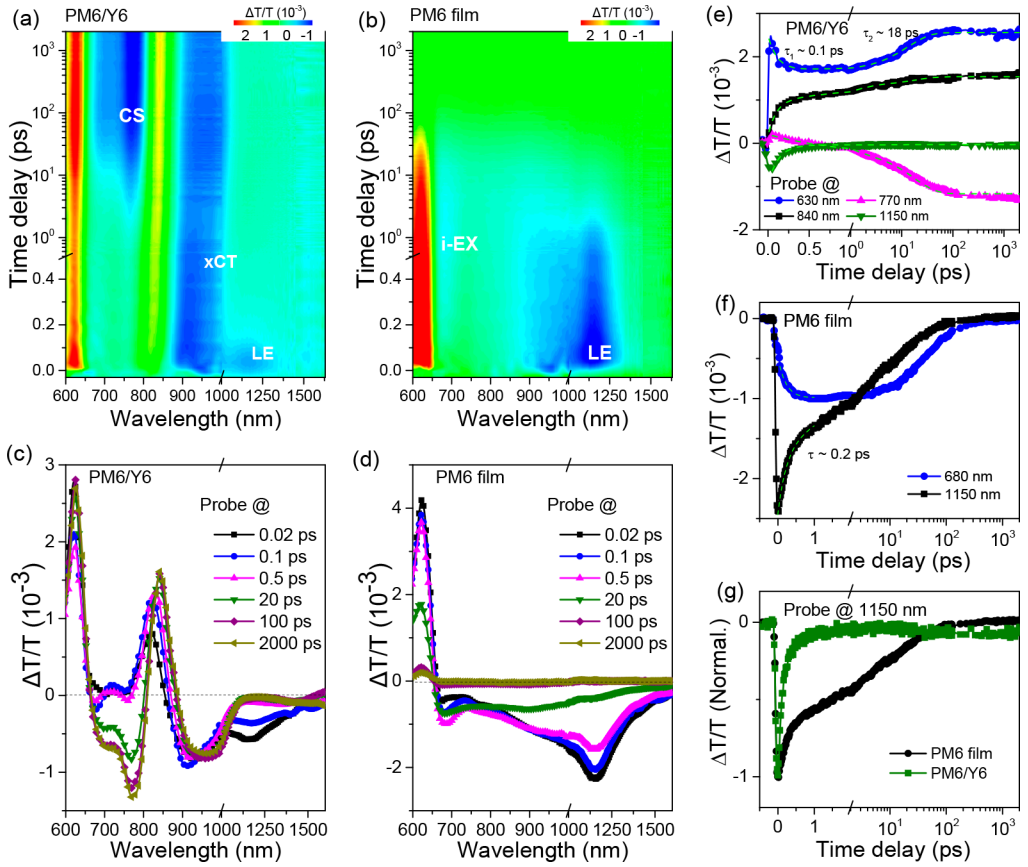

Figure 4. Electron transfer dynamics in the PM6/Y6 blend film. TA data recorded from the (a) PM6/Y6 blend and (b) neat PM6 films with pump at 550 nm. TA spectra recorded from the (c) PM6/Y6 blend and (d) neat PM6 films at different time delays. (e) TA traces probed at different wavelengths recorded from the blend PM6/Y6 film with pump at 550 nm. (f) TA traces of ESA signals probed at 680 and 1150 nm recorded from the neat PM6 film. (g) Normalized TA traces probed at 1150 nm recorded from the blend PM6/Y6 and neat PM6 films.

compared to that in the polymer/fullerene systems. This is consistent with literature results that the performance of OPV device is less sensitive to the annealing temperature.[5,60]

Electron Transfer Dynamics. Similar to conventional polymer/fullerene systems, electron transfer is an important channel for photocharge generation in OPV blends with NFAs.[29,64] However, whether the xCT-mediated charge generation mechanism established in polymer/fullerene blends applies to the OPV blends with NFAs remains to be determined. To clarify this issue, we probe the electron transfer channel of charge generation in PM6/Y6 blends by selectively exciting the polymer donor.

Figure 4a shows the TA data recorded from the blend PM6/Y6 film upon pump at 550 nm. Temporal evolution also exhibits two-stage dynamics (Figure 4a). Initially, the optical pump excites the LE state in PM6 with the ESA feature centered at 1150 nm. The final long-lived state shows the same spectrum as that of the CS state (Figure S9). Similar to hole transfer, an intermediate state is also involved in the electron transfer channel of charge separation. However, the spectral feature of the intermediate state is markedly different from that of any excited species in the neat PM6 film (Figure 4c and d). Polymer PM6 is a linear copolymer with alternating electron-donating and -withdrawing units, in which the excimer state can be formed with a certain degree of CT character. The LE state is partially converted to an excimer-like i-EX state in the neat polymer PM6 film with the ESA feature at 680 nm (Figure 4b, d, and f). However, the feature of such an i-EX state in PM6 is different from that of the intermediate state in the blend PM6/Y6 films. Notably, the onset of the intermediate state is accompanied by growth of the GSB signal of Y6 (Figure 4e), which suggests that electron transfer starts during the formation of the intermediate state. These results support that the intermediate step is an xCT state for the electron transfer channel of charge separation in the PM6/Y6 blend. The TA spectra of the xCT and CS states show similar bleach and ESA features but with a slight spectral shift, which is plausibly caused by the electro-absorption effect due to the increase of electron−hole separation distance during charge separation.[27,30,65] In addition, the signal of CS state exhibits increased magnitudes of the ESA feature near 770 nm and the bleach feature near 630 nm, which can be also explained by the modified electric field. The separate changes strongly modulate the optical response by influencing neighboring molecules as was previously observed in polymer/fullerene systems.[27,30,65]

The difference between the electron and hole transfer channels is also manifested in the decay dynamics of primarily excited LE states. Unlike the unchanged dynamics of LE at Y6 in the blend and neat Y6 samples, the LE state at PM6 decays much faster in the blend film than in the neat PM6 film (Figure 4c and d). The early stage lifetime of the LE state is shortened from ∼0.2 ps in the neat PM6 film to ∼0.1 ps in the blend (Figure 4e−g). A portion of bleach signal of Y6 acceptor is built up within the pulse duration, which is possibly due to the coherent electron transfer due to strong coupling between the

https://dx.doi.org/10.1021/jacs.0c04890
J. Am. Chem. Soc. 2020, 142, 12751−12759

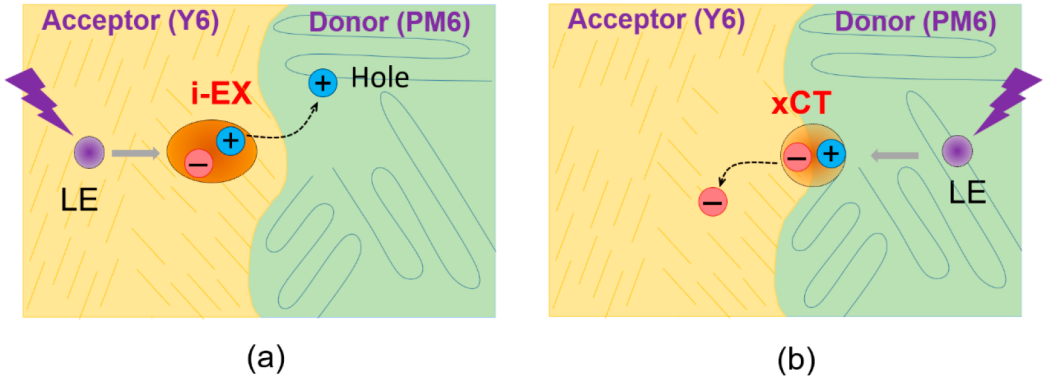

Figure 5. Schematic diagrams of the (a) hole transfer and (b) electron transfer channels of charge separation. When a photon is absorbed by acceptor Y6, the LE state at the acceptor site is separated into free polarons through the i-EX state as its intermediate step; when a photon is absorbed by donor PM6, the LE state at the donor site is separated into free polarons through the interfacial xCT state as its intermediate step.

LE and xCT states at the donor/acceptor interface.[30,38,66] In the blend, the LE state is directly converted into the intermediate xCT state prior to formation of the i-EX state in the PM6 moiety (Figure 4g). The electron transfer channel in the PM6/Y6 blend is regulated by the xCT-mediated scheme established in polymer/fullerene systems, the LE → xCT → CS pathway. During the xCT → CS process, the ESA signal in the range of 850−1000 nm shows a slight spectral shift, which is possibly caused by the absorption change that results from modification of the electron field by electron and hole polaron separation.[30]

DISCUSSION

Figure 5 compares the electron and hole transfer channels of charge separation in the PM6/Y6 blend and highlights the interplay between the i-EX and xCT states. Conversion from the photoexcited LE state to the i-EX state is observed in neat films of either polymer donor PM6 or small-molecule acceptor Y6. However, the role of such an intra-moiety state at PM6 and Y6 is markedly different for the electron and hole transfer channels of charge generation. The initial stage of charge separation is likely determined by competition between the LE → i-EX and LE → xCT pathways. In theory, the rate of the charge transfer process is highly sensitive to electronic coupling between the reactant and product states and the free Gibbs energy determined by the interfacial energetic offset.[28,67] For hole transfer, the small energy offset between the HOMO levels results in relatively slow formation of the xCT states at the donor/acceptor interface. Within the dimer structure of Y6 molecules, strong intermolecular interaction between the conjugation units with different electron affinities allows fast formation of the i-EX state from the LE state at Y6 (Figure 2f).[64] Consequently, the intra-moiety process of i-EX formation is more favorable than the interfacial hole transfer process to form the xCT state. The electron transfer channel shows a significantly different feature. Polymer donor PM6 is a copolymer with heterogeneous interchain and intrachain interactions between the conjugation units. A portion of the photoexcited LE state is converted into the excimer-like i-EX state in neat polymer PM6 (Figure 4f). However, formation of the xCT state is more favorable due to the interfacial energy offset between the LUMO levels being sufficiently high. These effects ensure that formation of the xCT state through interfacial electron transfer is more favorable than the intra-moiety process of i-EX state formation. The pathways involving different intermediate states in the polymer/NFA blend are fundamentally determined by the energy landscape and electronic coupling between different local and CT excitation species.

The intermediate i-EX state of the hole transfer channel is markedly different from the intermediate xCT state of the electron transfer channel. However, charge separation from these intermediate states occurs on a similar time scale (~15 ps for hole transfer and ~18 ps for electron transfer). The similar dissociation time scales of these bound intermediate states are possibly driven by similar charge hopping processes.[68−70] For more insights, we performed temperature-dependent measurements on the hole transfer dynamics (Figure S10). The correlated temperature dependences of the dynamics probed at 770 and 1550 nm confirm the major pathway of the dissociation of i-EX state for the hole transfer channel of charge separation. With increasing temperature from 200 to 300 K, the rate of charge separation increases gradually (Figure S10), which suggests that the thermal activation is an important driving force for charge separation in the PM6/Y6 blend. While more in-depth studies are necessary to fully elucidate the exact microscopic picture, we discuss a possible mechanism underlying the hole transfer channel mediated by the i-EX state. The pathway of the hole transfer without involving the CT state is possibly related to the nature of the i-EX state arising from the molecular packing in the Y6 domains. Experimental and quantum computational data suggest that Y6 molecules tend to form ordered aggregates of dimers.[59−61] Such a structure is plausibly beneficial for spatial extension of i-EX state with mixed LE and CT characters,[63,71] which results in a relatively longer spatial separation between electron and hole.[63,71] In this case, the thermal hopping at the donor/acceptor interface enables the escape of polarons from the Coulomb potential without passing through the bound xCT state.

The i-EX state-mediated scenario explains the efficient hole transfer with a small HOMO energy offset between the donor and acceptor in OPV devices with NFAs. The formation of such an i-EX state in the Y6 moiety is independent of the energy offset between HOMO levels and electronic coupling at the donor/acceptor interface. Such a feature avoids the interfacial energy loss during the formation of the interfacial CT state through the electron transfer process as was commonly observed in polymer/fullerene systems, which is plausibly a key factor for the high photocurrent density and

https://dx.doi.org/10.1021/jacs.0c04890
J. Am. Chem. Soc. 2020, 142, 12751−12759

high open-circuit voltage recently demonstrated in these Y6-based OPV devices. The intra-moiety state is mainly regulated by the interaction between different Y6 molecules, which probably arises from the nonzero molecular dipole caused by the axisymmetric structure and face-to-face $\pi-\pi$ stacking of the Y6 dimer. The lamella structure of the Y6 dimer is possibly beneficial for exciton delocalization to obtain charge separation with a small interfacial energy loss.[72] To uncover the exact nature of the i-EX state, further effort is required to study whether it is a CT state in the dimer configuration or an excimer-like state from the hybridization of LE and CT characters.

CONCLUSION

In summary, we have identified an i-EX state as the intermediate step for the hole transfer channel of photocharge generation in the PM6/Y6 blend film. The photoexcited LE state at NFA Y6 is converted into an intermediate i-EX state (<0.2 ps) that further dissociated into the CS state of free polarons (~15 ps). Such an intra-moiety state, with electrons and holes localized at the same moiety of the Y6 acceptor, is markedly different from the intermediate xCT state of the electron transfer channel previously established in polymer/fullerene systems. Because of intermolecular coupling in the Y6 moiety, i-EX state formation is independent of the energy alignment and electron coupling at the donor/acceptor interface, which explains the highly efficient hole transfer with small HOMO energy offset in OPV blends with NFAs. The unprecedented role of the i-EX state in charge generation elucidated herein suggests an alternative strategy by manipulating the intra-moiety molecular interaction toward optimizing the energy landscape and electron coupling between the i-EX state and other excited species for further improvement of OPV devices.

ASSOCIATED CONTENT

Supporting Information

The Supporting Information is available free of charge at https://pubs.acs.org/doi/10.1021/jacs.0c04890.

Additional experimental details; device performance characterization; absorption and photoluminescence spectra of solution and film Y6 samples; pump wavelength selection for TA measurements; excitation fluence-dependent TA measurements; TA measurements of a solution Y6 sample; pump wavelength-dependent measurements; annealing effects; spectral characteristics of the CS state; and temperature-dependent measurements (PDF)

AUTHOR INFORMATION

Corresponding Author

Chunfeng Zhang − *National Laboratory of Solid State Microstructures, School of Physics, and Collaborative Innovation Center for Advanced Microstructures, Nanjing University, Nanjing 210093, China;* orcid.org/0000-0001-9030-5606; Email: cfzhang@nju.edu.cn

Authors

Rui Wang − *National Laboratory of Solid State Microstructures, School of Physics, and Collaborative Innovation Center for Advanced Microstructures, Nanjing University, Nanjing 210093, China*

Qian Li − *National Laboratory of Solid State Microstructures, School of Physics, and Collaborative Innovation Center for Advanced Microstructures, Nanjing University, Nanjing 210093, China*

Zhiguo Zhang − *College of Materials Science and Engineering, Beijing University of Chemical Technology, Beijing 100029, China;* orcid.org/0000-0003-4341-7773

Xiaoyong Wang − *National Laboratory of Solid State Microstructures, School of Physics, and Collaborative Innovation Center for Advanced Microstructures, Nanjing University, Nanjing 210093, China;* orcid.org/0000-0003-1147-0051

Min Xiao − *National Laboratory of Solid State Microstructures, School of Physics, and Collaborative Innovation Center for Advanced Microstructures, Nanjing University, Nanjing 210093, China; Department of Physics, University of Arkansas, Fayetteville, Arkansas 72701, United States*

Complete contact information is available at: https://pubs.acs.org/10.1021/jacs.0c04890

Notes

The authors declare no competing financial interest.

ACKNOWLEDGMENTS

This work is supported by the National Key R&D Program of China (grant nos. 2018YFA0209101 and 2017YFA0303700), the National Science Foundation of China (grant nos. 21922302, 21873047, 11904168, 91833305, and 91850105), the Science and Technology Project of Jiangsu Province of China (BK20190290), the Priority Academic Program Development of Jiangsu Higher Education Institutions (PAPD), and the Fundamental Research Funds for the Central University. We acknowledge Dr. Xuewei Wu for providing technical assistance.

REFERENCES

(1) Best Research-Cell Efficiency Chart; https://www.nrel.gov/pv/cell-efficiency.html.

(2) Cui, Y.; Yao, H. F.; Zhang, J. Q.; Xian, K. H.; Zhang, T.; Hong, L.; Wang, Y. M.; Xu, Y.; Ma, K. Q.; An, C. B.; He, C.; Wei, Z. X.; Gao, F.; Hou, J. H. Single-Junction Organic Photovoltaic Cells with Approaching 18% Efficiency. *Adv. Mater.* **2020**, *32*, 1908205.

(3) Lin, Y.; Wang, J.; Zhang, Z. G.; Bai, H.; Li, Y.; Zhu, D.; Zhan, X. An Electron Acceptor Challenging Fullerenes for Efficient Polymer Solar Cells. *Adv. Mater.* **2015**, *27*, 1170.

(4) Holliday, S.; Ashraf, R. S.; Wadsworth, A.; Baran, D.; Yousaf, S. A.; Nielsen, C. B.; Tan, C. H.; Dimitrov, S. D.; Shang, Z. R.; Gasparini, N.; Alamoudi, M.; Laquai, F.; Brabec, C. J.; Salleo, A.; Durrant, J. R.; McCulloch, I. High-Efficiency and Air-Stable P3ht-Based Polymer Solar Cells with a New Non-Fullerene Acceptor. *Nat. Commun.* **2016**, *7*, 11585.

(5) Yuan, J.; Zhang, Y.; Zhou, L.; Zhang, G.; Yip, H.-L.; Lau, T.-K.; Lu, X.; Zhu, C.; Peng, H.; Johnson, P. A.; Leclerc, M.; Cao, Y.; Ulanski, J.; Li, Y.; Zou, Y. Single-Junction Organic Solar Cell with over 15% Efficiency Using Fused-Ring Acceptor with Electron-Deficient Core. *Joule* **2019**, *3*, 1140.

(6) Yuan, J.; Huang, T.; Cheng, P.; Zou, Y.; Zhang, H.; Yang, J. L.; Chang, S. Y.; Zhang, Z.; Huang, W.; Wang, R.; Meng, D.; Gao, F.; Yang, Y. Enabling Low Voltage Losses and High Photocurrent in Fullerene-Free Organic Photovoltaics. *Nat. Commun.* **2019**, *10*, 570.

(7) Cui, Y.; Yao, H.; Zhang, J.; Zhang, T.; Wang, Y.; Hong, L.; Xian, K.; Xu, B.; Zhang, S.; Peng, J.; Wei, Z.; Gao, F.; Hou, J. Over 16% Efficiency Organic Photovoltaic Cells Enabled by a Chlorinated Acceptor with Increased Open-Circuit Voltages. *Nat. Commun.* **2019**, *10*, 2515.

(8) Meng, L.; Zhang, Y.; Wan, X.; Li, C.; Zhang, X.; Wang, Y.; Ke, X.; Xiao, Z.; Ding, L.; Xia, R. Organic and Solution-Processed Tandem Solar Cells with 17.3% Efficiency. *Science* **2018**, *361*, 1094.
(9) Bin, H.; Gao, L.; Zhang, Z.-G.; Yang, Y.; Zhang, Y.; Zhang, C.; Chen, S.; Xue, L.; Yang, C.; Xiao, M.; Li, Y. 11.4% Efficiency Non-Fullerene Polymer Solar Cells with Trialkylsilyl Substituted 2d-Conjugated Polymer as Donor. *Nat. Commun.* **2016**, *7*, 13651.
(10) Wadsworth, A.; Moser, M.; Marks, A.; Little, M. S.; Gasparini, N.; Brabec, C. J.; Baran, D.; McCulloch, I. Critical Review of the Molecular Design Progress in Non-Fullerene Electron Acceptors Towards Commercially Viable Organic Solar Cells. *Chem. Soc. Rev.* **2019**, *48*, 1596.
(11) Zhang, G.; Zhao, J.; Chow, P. C. Y.; Jiang, K.; Zhang, J.; Zhu, Z.; Zhang, J.; Huang, F.; Yan, H. Nonfullerene Acceptor Molecules for Bulk Heterojunction Organic Solar Cells. *Chem. Rev.* **2018**, *118*, 3447.
(12) Hou, J.; Inganas, O.; Friend, R. H.; Gao, F. Organic Solar Cells Based on Non-Fullerene Acceptors. *Nat. Mater.* **2018**, *17*, 119.
(13) Cheng, P.; Li, G.; Zhan, X.; Yang, Y. Next-Generation Organic Photovoltaics Based on Non-Fullerene Acceptors. *Nat. Photonics* **2018**, *12*, 131.
(14) Yan, C.; Barlow, S.; Wang, Z.; Yan, H.; Jen, A. K. Y.; Marder, S. R.; Zhan, X. Non-Fullerene Acceptors for Organic Solar Cells. *Nat. Rev. Mater.* **2018**, *3*, 18003.
(15) Wang, R.; Yuan, J.; Wang, R.; Han, G.; Huang, T.; Huang, W.; Xue, J.; Wang, H. C.; Zhang, C.; Zhu, C.; Cheng, P.; Meng, D.; Yi, Y.; Wei, K. H.; Zou, Y.; Yang, Y. Rational Tuning of Molecular Interaction and Energy Level Alignment Enables High-Performance Organic Photovoltaics. *Adv. Mater.* **2019**, *31*, e1904215.
(16) Chen, S.; Liu, Y.; Zhang, L.; Chow, P. C. Y.; Wang, Z.; Zhang, G.; Ma, W.; Yan, H. A Wide-Bandgap Donor Polymer for Highly Efficient Non-Fullerene Organic Solar Cells with a Small Voltage Loss. *J. Am. Chem. Soc.* **2017**, *139*, 6298.
(17) Zhang, J.; Tan, H. S.; Guo, X.; Facchetti, A.; Yan, H. Material Insights and Challenges for Non-Fullerene Organic Solar Cells Based on Small Molecular Acceptors. *Nat. Energy* **2018**, *3*, 720.
(18) Yu, G.; Gao, J.; Hummelen, J. C.; Wudl, F.; Heeger, A. J. Polymer Photovoltaic Cells - Enhanced Efficiencies Via a Network of Internal Donor-Acceptor Heterojunctions. *Science* **1995**, *270*, 1789.
(19) Halls, J. J. M.; Walsh, C. A.; Greenham, N. C.; Marseglia, E. A.; Friend, R. H.; Moratti, S. C.; Holmes, A. B. Efficient Photodiodes from Interpenetrating Polymer Networks. *Nature* **1995**, *376*, 498.
(20) Stoltzfus, D. M.; Donaghey, J. E.; Armin, A.; Shaw, P. E.; Burn, P. L.; Meredith, P. Charge Generation Pathways in Organic Solar Cells: Assessing the Contribution from the Electron Acceptor. *Chem. Rev.* **2016**, *116*, 12920.
(21) Clarke, T. M.; Durrant, J. R. Charge Photogeneration in Organic Solar Cells. *Chem. Rev.* **2010**, *110*, 6736.
(22) Qian, D.; Zheng, Z.; Yao, H.; Tress, W.; Hopper, T. R.; Chen, S.; Li, S.; Liu, J.; Chen, S.; Zhang, J.; Liu, X.-K.; Gao, B.; Ouyang, L.; Jin, Y.; Pozina, G.; Buyanova, I. A.; Chen, W. M.; Inganas, O.; Coropceanu, V.; Bredas, J.-L.; Yan, H.; Hou, J.; Zhang, F.; Bakulin, A. A.; Gao, F. Design Rules for Minimizing Voltage Losses in High-Efficiency Organic Solar Cells. *Nat. Mater.* **2018**, *17*, 703.
(23) Etzold, F.; Howard, I. A.; Mauer, R.; Meister, M.; Kim, T.-D.; Lee, K.-S.; Baek, N. S.; Laquai, F. Ultrafast Exciton Dissociation Followed by Nongeminate Charge Recombination in Pcdtbt:Pcbm Photovoltaic Blends. *J. Am. Chem. Soc.* **2011**, *133*, 9469.
(24) Ohkita, H.; Cook, S.; Astuti, Y.; Duffy, W.; Tierney, S.; Zhang, W.; Heeney, M.; McCulloch, I.; Nelson, J.; Bradley, D. D. C.; Durrant, J. R. Charge Carrier Formation in Polythiophene/Fullerene Blend Films Studied by Transient Absorption Spectroscopy. *J. Am. Chem. Soc.* **2008**, *130*, 3030.
(25) Savoie, B. M.; Rao, A.; Bakulin, A. A.; Gelinas, S.; Movaghar, B.; Friend, R. H.; Marks, T. J.; Ratner, M. A. Unequal Partnership: Asymmetric Roles of Polymeric Donor and Fullerene Acceptor in Generating Free Charge. *J. Am. Chem. Soc.* **2014**, *136*, 2876.
(26) Jailaubekov, A. E.; Willard, A. P.; Tritsch, J. R.; Chan, W.-L.; Sai, N.; Gearba, R.; Kaake, L. G.; Williams, K. J.; Leung, K.; Rossky, P. J.; Zhu, X. Y. Hot Charge-Transfer Excitons Set the Time Limit for Charge Separation at Donor/Acceptor Interfaces in Organic Photovoltaics. *Nat. Mater.* **2013**, *12*, 66.
(27) Menke, S. M.; Cheminal, A.; Conaghan, P.; Ran, N. A.; Greehnam, N. C.; Bazan, G. C.; Nguyen, T. Q.; Rao, A.; Friend, R. H. Order Enables Efficient Electron-Hole Separation at an Organic Heterojunction with a Small Energy Loss. *Nat. Commun.* **2018**, *8*, 277.
(28) Jakowetz, A. C.; Bohm, M. L.; Zhang, J.; Sadhanala, A.; Huettner, S.; Bakulin, A. A.; Rao, A.; Friend, R. H. What Controls the Rate of Ultrafast Charge Transfer and Charge Separation Efficiency in Organic Photovoltaic Blends. *J. Am. Chem. Soc.* **2016**, *138*, 11672.
(29) Bakulin, A. A.; Rao, A.; Pavelyev, V. G.; van Loosdrecht, P. H. M.; Pshenichnikov, M. S.; Niedzialek, D.; Cornil, J.; Beljonne, D.; Friend, R. H. The Role of Driving Energy and Delocalized States for Charge Separation in Organic Semiconductors. *Science* **2012**, *335*, 1340.
(30) Gelinas, S.; Rao, A.; Kumar, A.; Smith, S. L.; Chin, A. W.; Clark, J.; van der Poll, T. S.; Bazan, G. C.; Friend, R. H. Ultrafast Long-Range Charge Separation in Organic Semiconductor Photovoltaic Diodes. *Science* **2014**, *343*, 512.
(31) Baran, D.; Gasparini, N.; Wadsworth, A.; Tan, C. H.; Wehbe, N.; Song, X.; Hamid, Z.; Zhang, W.; Neophytou, M.; Kirchartz, T.; Brabec, C. J.; Durrant, J. R.; McCulloch, I. Robust Nonfullerene Solar Cells Approaching Unity External Quantum Efficiency Enabled by Suppression of Geminate Recombination. *Nat. Commun.* **2018**, *9*, 2059.
(32) Guo, J.; Ohkita, H.; Benten, H.; Ito, S. Charge Generation and Recombination Dynamics in Poly(3-Hexylthiophene)/Fullerene Blend Films with Different Regioregularities and Morphologies. *J. Am. Chem. Soc.* **2010**, *132*, 6154.
(33) Guo, J.; Ohkita, H.; Benten, H.; Ito, S. Near-Ir Femtosecond Transient Absorption Spectroscopy of Ultrafast Polaron and Triplet Exciton Formation in Polythiophene Films with Different Regioregularities. *J. Am. Chem. Soc.* **2009**, *131*, 16869.
(34) Bin, H.; Yang, Y.; Zhang, Z.-G.; Ye, L.; Ghasem, M.; Chen, S.; Zhang, Y.; Zhang, C.; Sun, C.; Xue, L.; Yang, C.; Ade, H.; Li, Y. 9.73% Efficiency Nonfullerene All Organic Small Molecule Solar Cells with Absorption-Complementary Donor and Acceptor. *J. Am. Chem. Soc.* **2017**, *139*, 5085.
(35) Sun, C.; Qin, S.; Wang, R.; Chen, S.; Pan, F.; Qiu, B.; Shang, Z.; Meng, L.; Zhang, C.; Xiao, M.; Yang, C.; Li, Y. High Efficiency Polymer Solar Cells with Efficient Hole Transfer at Zero Highest Occupied Molecular Orbital Offset between Methylated Polymer Donor and Brominated Acceptor. *J. Am. Chem. Soc.* **2020**, *142*, 1465.
(36) Luo, Z.; Bin, H.; Liu, T.; Zhang, Z. G.; Yang, Y.; Zhong, C.; Qiu, B.; Li, G.; Gao, W.; Xie, D.; Wu, K.; Sun, Y.; Liu, F.; Li, Y.; Yang, C. Fine-Tuning of Molecular Packing and Energy Level through Methyl Substitution Enabling Excellent Small Molecule Acceptors for Nonfullerene Polymer Solar Cells with Efficiency up to 12.54%. *Adv. Mater.* **2018**, *30*, 1706124.
(37) Liu, J.; Chen, S.; Qian, D.; Gautam, B.; Yang, G.; Zhao, J.; Bergqvist, J.; Zhang, F.; Ma, W.; Ade, H.; Inganas, O.; Gundogdu, K.; Gao, F.; Yan, H. Fast Charge Separation in a Non-Fullerene Organic Solar Cell with a Small Driving Force. *Nat. Energy* **2016**, *1*, 16809.
(38) Falke, S. M.; Rozzi, C. A.; Brida, D.; Maiuri, M.; Amato, M.; Sommer, E.; De Sio, A.; Rubio, A.; Cerullo, G.; Molinari, E.; Lienau, C. Coherent Ultrafast Charge Transfer in an Organic Photovoltaic Blend. *Science* **2014**, *344*, 1001.
(39) Tautz, R.; Da Como, E.; Wiebeler, C.; Soavi, G.; Dumsch, I.; Froehlich, N.; Grancini, G.; Allard, S.; Scherf, U.; Cerullo, G.; Schumacher, S.; Feldmann, J. Charge Photogeneration in Donor-Acceptor Conjugated Materials: Influence of Excess Excitation Energy and Chain Length. *J. Am. Chem. Soc.* **2013**, *135*, 4282.
(40) Monahan, N. R.; Williams, K. W.; Kumar, B.; Nuckolls, C.; Zhu, X.-Y. Direct Observation of Entropy-Driven Electron-Hole Pair Separation at an Organic Semiconductor Interface. *Phys. Rev. Lett.* **2015**, *114*, 247003.
(41) Hood, S. N.; Kassal, I. Entropy and Disorder Enable Charge Separation in Organic Solar Cells. *J. Phys. Chem. Lett.* **2016**, *7*, 4495.

https://dx.doi.org/10.1021/jacs.0c04890
J. Am. Chem. Soc. 2020, 142, 12751−12759

(42) Gregg, B. A. Entropy of Charge Separation in Organic Photovoltaic Cells: The Benefit of Higher Dimensionality. *J. Phys. Chem. Lett.* **2011**, *2*, 3013.
(43) Hestand, N. J.; Kazantsev, R. V.; Weingarten, A. S.; Palmer, L. C.; Stupp, S. I.; Spano, F. C. Extended-Charge-Transfer Excitons in Crystalline Supramolecular Photocatalytic Scaffolds. *J. Am. Chem. Soc.* **2016**, *138*, 11762.
(44) Stein, T.; Kronik, L.; Baer, R. Reliable Prediction of Charge Transfer Excitations in Molecular Complexes Using Time-Dependent Density Functional Theory. *J. Am. Chem. Soc.* **2009**, *131*, 2818.
(45) Guo, Z.; Lee, D.; Schaller, R. D.; Zuo, X.; Lee, B.; Luo, T.; Gao, H.; Huang, L. Relationship between Interchain Interaction, Exciton Delocalization, and Charge Separation in Low-Bandgap Copolymer Blends. *J. Am. Chem. Soc.* **2014**, *136*, 10024.
(46) Jenekhe, S. A.; Osaheni, J. A. Excimers and Exciplexes of Conjugated Polymers. *Science* **1994**, *265*, 765.
(47) Reid, O. G.; Pensack, R. D.; Song, Y.; Scholes, G. D.; Rumbles, G. Charge Photogeneration in Neat Conjugated Polymers. *Chem. Mater.* **2014**, *26*, 561.
(48) Rolczynski, B. S.; Szarko, J. M.; Son, H. J.; Liang, Y.; Yu, L.; Chen, L. X. Ultrafast Intramolecular Exciton Splitting Dynamics in Isolated Low-Band-Gap Polymers and Their Implication in Photovoltaic Materials Design. *J. Am. Chem. Soc.* **2012**, *134*, 4142.
(49) De Sio, A.; Troiani, F.; Maiuri, M.; Rehault, J.; Sommer, E.; Lim, J.; Huelga, S. F.; Plenio, M. B.; Rozzi, C. A.; Cerullo, G.; Molinari, E.; Lienau, C. Tracking the Coherent Generation of Polaron Pairs in Conjugated Polymers. *Nat. Commun.* **2016**, *7*, 13742.
(50) Di Nuzzo, D.; Viola, D.; Fischer, F. S.; Cerullo, G.; Ludwigs, S.; Da Como, E. Enhanced Photogeneration of Polaron Pairs in Neat Semicrystalline Donor-Acceptor Copolymer Films Via Direct Excitation of Interchain Aggregates. *J. Phys. Chem. Lett.* **2015**, *6*, 1196.
(51) Wang, R.; Yao, Y.; Zhang, C.; Zhang, Y.; Bin, H.; Xue, L.; Zhang, Z. G.; Xie, X.; Ma, H.; Wang, X.; Li, Y.; Xiao, M. Ultrafast Hole Transfer Mediated by Polaron Pairs in All-Polymer Photovoltaic Blends. *Nat. Commun.* **2019**, *10*, 398.
(52) An, Z.; Wu, C. Q.; Sun, X. Dynamics of Photogenerated Polarons in Conjugated Polymers. *Phys. Rev. Lett.* **2004**, *93*, 216407.
(53) Yan, T.; Song, W.; Huang, J.; Peng, R.; Huang, L.; Ge, Z. 16.67% Rigid and 14.06% Flexible Organic Solar Cells Enabled by Ternary Heterojunction Strategy. *Adv. Mater.* **2019**, *31*, 1902210.
(54) Yu, R.; Yao, H.; Cui, Y.; Hong, L.; He, C.; Hou, J. Improved Charge Transport and Reduced Nonradiative Energy Loss Enable over 16% Efficiency in Ternary Polymer Solar Cells. *Adv. Mater.* **2019**, *31*, 1902302.
(55) Lee, C.-L.; Hwang, I.-W.; Byeon, C. C.; Kim, B. H.; Greenham, N. C. Triplet Exciton and Polaron Dynamics in Phosphorescent Dye Blended Polymer Photovoltaic Devices. *Adv. Funct. Mater.* **2010**, *20*, 2945.
(56) Schlenker, C. W.; Chen, K. S.; Yip, H. L.; Li, C. Z.; Bradshaw, L. R.; Ochsenbein, S. T.; Ding, F.; Li, X. S.; Gamelin, D. R.; Jen, A. K.; Ginger, D. S. Polymer Triplet Energy Levels Need Not Limit Photocurrent Collection in Organic Solar Cells. *J. Am. Chem. Soc.* **2012**, *134*, 19661.
(57) Ginger, D. S.; Greenham, N. C. Photoinduced Electron Transfer from Conjugated Polymers to Cdse Nanocrystals. *Phys. Rev. B: Condens. Matter Mater. Phys.* **1999**, *59*, 10622.
(58) Rao, A.; Chow, P. C.; Gelinas, S.; Schlenker, C. W.; Li, C. Z.; Yip, H. L.; Jen, A. K.; Ginger, D. S.; Friend, R. H. The Role of Spin in the Kinetic Control of Recombination in Organic Photovoltaics. *Nature* **2013**, *500*, 435.
(59) Perdigón-Toro, L.; Zhang, H.; Markina, A.; Yuan, J.; Hosseini, S. M.; Wolff, C. M.; Zuo, G.; Stolterfoht, M.; Zou, Y.; Gao, F. Barrierless Free Charge Generation in the High-Performance Pm6: Y6 Bulk Heterojunction Non-Fullerene Solar Cell. *Adv. Mater.* **2020**, *32*, 1906763.
(60) Zhu, L.; Zhang, M.; Zhou, G.; Hao, T.; Xu, J.; Wang, J.; Qiu, C.; Prine, N.; Ali, J.; Feng, W.; Gu, X.; Ma, Z.; Tang, Z.; Zhu, H.; Ying, L.; Zhang, Y.; Liu, F. Efficient Organic Solar Cell with 16.88% Efficiency Enabled by Refined Acceptor Crystallization and Morphology with Improved Charge Transfer and Transport Properties. *Adv. Energy Mater.* **2020**, *10*, 1904234.
(61) Xiao, C.; Li, C.; Liu, F.; Zhang, L.; Li, W. Single-Crystal Field-Effect Transistors Based on a Fused-Ring Electron Acceptor with High Ambipolar Mobilities. *J. Mater. Chem. C* **2020**, *8*, 5370.
(62) Chandross, E. A.; Ferguson, J. Mixed Excimer Fluorescence; the Importance of Charge-Transfer Interaction. *J. Chem. Phys.* **1967**, *47*, 2557.
(63) Hestand, N. J.; Spano, F. C. Expanded Theory of H- and J-Molecular Aggregates: The Effects of Vibronic Coupling and Intermolecular Charge Transfer. *Chem. Rev.* **2018**, *118*, 7069.
(64) Eisner, F. D.; Azzouzi, M.; Fei, Z.; Hou, X.; Anthopoulos, T. D.; Dennis, T. J. S.; Heeney, M.; Nelson, J. Hybridization of Local Exciton and Charge-Transfer States Reduces Nonradiative Voltage Losses in Organic Solar Cells. *J. Am. Chem. Soc.* **2019**, *141*, 6362.
(65) Jakowetz, A. C.; Boehm, M. L.; Sadhanala, A.; Huettner, S.; Rao, A.; Friend, R. H. Visualizing Excitations at Buried Heterojunctions in Organic Semiconductor Blends. *Nat. Mater.* **2017**, *16*, 551.
(66) Tamai, Y.; Fan, Y.; Kim, V. O.; Ziabrev, K.; Rao, A.; Barlow, S.; Marder, S. R.; Friend, R. H.; Menke, S. M. Ultrafast Long-Range Charge Separation in Nonfullerene Organic Solar Cells. *ACS Nano* **2017**, *11*, 12473.
(67) Eastham, N. D.; Logsdon, J. L.; Manley, E. F.; Aldrich, T. J.; Leonardi, M. J.; Wang, G.; Powers-Riggs, N. E.; Young, R. M.; Chen, L. X.; Wasielewski, M. R.; Melkonyan, F. S.; Chang, R. P. H.; Marks, T. J. Hole-Transfer Dependence on Blend Morphology and Energy Level Alignment in Polymer: Itic Photovoltaic Materials. *Adv. Mater.* **2018**, *30*, 1704263.
(68) Athanasopoulos, S.; Tscheuschner, S.; Bässler, H.; Köhler, A. Efficient Charge Separation of Cold Charge-Transfer States in Organic Solar Cells through Incoherent Hopping. *J. Phys. Chem. Lett.* **2017**, *8*, 2093.
(69) Vandewal, K.; Albrecht, S.; Hoke, E. T.; Graham, K. R.; Widmer, J.; Douglas, J. D.; Schubert, M.; Mateker, W. R.; Bloking, J. T.; Burkhard, G. F.; Sellinger, A.; Fréchet, J. M. J.; Amassian, A.; Riede, M. K.; McGehee, M. D.; Neher, D.; Salleo, A. Efficient Charge Generation by Relaxed Charge-Transfer States at Organic Interfaces. *Nat. Mater.* **2014**, *13*, 63.
(70) Gao, F.; Tress, W.; Wang, J.; Inganas, O. Temperature Dependence of Charge Carrier Generation in Organic Photovoltaics. *Phys. Rev. Lett.* **2015**, *114*, 128701.
(71) Hestand, N. J.; Kazantsev, R. V.; Weingarten, A. S.; Palmer, L. C.; Stupp, S. I.; Spano, F. C. Extended-Charge-Transfer Excitons in Crystalline Supramolecular Photocatalytic Scaffolds. *J. Am. Chem. Soc.* **2016**, *138*, 11762.
(72) Apperloo, J. J.; Janssen, R. A.; Malenfant, P. R.; Fréchet, J. M. Interchain Delocalization of Photoinduced Neutral and Charged States in Nanoaggregates of Lengthy Oligothiophenes. *J. Am. Chem. Soc.* **2001**, *123*, 6916.

https://dx.doi.org/10.1021/jacs.0c04890
J. Am. Chem. Soc. 2020, 142, 12751−12759